Atomic Layer Deposition of Polyimide on Microporous Polyethersulfone Membranes for Enhanced and Tunable Performances

Ting Sheng, He Chen, Sen Xiong, Xiaoqiang Chen, and Yong Wang
State Key Laboratory of Materials-Oriented Chemical Engineering, College of Chemistry and Chemical Engineering, Nanjing Tech University (Formerly Nanjing University of Technology), Nanjing 210009 P.R. China

DOI 10.1002/aic.14553
Published online July 10, 2014 in Wiley Online Library (wileyonlinelibrary.com)

Atomic layer deposition (ALD) of polyimide (PI) is explored to tune the separation properties of microporous polyethersulfone (PES) membranes and also to improve their mechanic and thermal stability. Conformal and uniform thin layers of PI are deposited along the pore wall throughout the entire PES membrane instead of forming a top layer merely on the membrane surface. With increasing ALD cycles, the pore size of the PES membrane is progressively reduced, leading to increased retention. The permeation is correspondingly decreased but its drop is less pronounced than the increase of retention. For example, the retention to 23-nm silica nanospheres is significantly increased from nearly zero to 60% after 3000 ALD cycles, whereas the water flux is moderately decreased by 54%. Moreover, ALD of PI evidently enhances the mechanical strength and thermal resistance of the PES membrane as PI tightly wraps the skeleton of the membrane. © 2014 American Institute of Chemical Engineers *AIChE J*, 60: 3614–3622, 2014
Keywords: atomic layer deposition, membranes, modification, polyethersulfone, polyimide

Introduction

Membrane-based separation is playing an increasingly important role in a diversity of fields related to water, energy, environment, and natural resources where the size-sieving mechanism governs the separation process.[1,2] The performance of a membrane is mainly dictated by the pore structure, chemistry, and physical properties of the membrane.[3,4] There is a constant demand for membranes with better permselectivity as well as enhanced chemical and physical stabilities to reduce the operation costs and to be used in harsh conditions. Therefore, huge efforts have been invested in exploring new membrane-forming materials and processes, for example, carbon nanotubes,[5] graphene,[6] block copolymers,[7] metal-organic frameworks,[8] chemical vapor deposition (CVD),[9] and layer-by-layer deposition.[10] Alternatively, modification on traditionally used materials is also demonstrated to be an efficient and affordable way to upgrade membrane performances.[11]

Atomic layer deposition (ALD), which is previously predominantly used in the field of microelectronics,[12–14] has been newly adopted to modify and functionalize separation membranes.[15–18] ALD is based on the self-limited surface reactions between precursors. It is distinguished from other deposition techniques for its uniform and conformal deposition of materials exclusively on the substrate surface (including internal surfaces of porous substrates) and the atomic level control of the thickness of the deposition layer.[19–22] Moreover, as precursors for ALD are exposed to the substrate in the vaporized state, ALD is particularly suited for the homogeneous deposition of porous media with fine porosities, for example, membranes. In clear contrast, the sol-gel method based on liquid-phase reactions is frequently suffering from clogging fine pores or inhomogeneous coating because of capillarity or diffusion problems. ALD has been recently used to modify membranes with various chemical properties and pore structures including polymeric membranes[15–17] and inorganic membranes[18] with pore sizes ranged from a few nanometers to submicrometers. The function of ALD modification on membranes is multiple: (1) to precisely tune the pore size by altering the thickness of the deposition layer, (2) to improve the surface hydrophilicity and consequently the fouling resistance by covering the membrane surface with a highly hydrophilic oxide layer, (3) to enhance the chemical and thermal stability by taking the advantage of the barrier effect of the deposited oxide layer, and other functions specific to the substrate membranes.

Up to now only metal oxides, mainly aluminum oxide and titanium oxide, are ALD-deposited on membranes to deliver a modification effect. In some cases, deposition of metal oxides on a specific membrane might not be the best choice. For example, polymeric membranes deposited with a thick layer of metal oxide may become brittle and the large difference in the thermal expansion between the polymeric substrate and the deposited inorganic layer may cause deformation or even failure of the membrane when used at elevated temperatures. ALD of polymers is expected to provide a solution to this challenge. It was demonstrated very recently that polyimide (PI) can also be produced by the

Correspondence concerning this article should be addressed to Y. Wang at yongwang@njtech.edu.cn

condensation polymerization between dianhydrides and diamines in the ALD mode.[23,24] Moreover, PI, as a high-performance engineering plastic, is well-known for its outstanding mechanical strength, thermal resistance, and chemical stability,[25] and it has long been used to produce membranes for gas separation,[26,27] solvent-resistant nanofiltration,[28,29] and pervaporation.[30] Therefore, there might be a chance to ALD-deposit PI on membranes, especially polymeric membranes, to tune their properties and to upgrade their performances.

In this study, we demonstrate, for the first time, the deposition of PI on microporous polyethersulfone (PES) membranes in the ALD mode. PES membranes are screened to use as the substrates because of the following reasons. First, PES membranes are a popular type of membranes and extensively used in microfiltration and ultrafiltraion.[31,32] Second, PES also possesses a good thermal resistance allowing it to tolerate the deposition temperature needed for the ALD of PI.[33] Third, PES has a good compatibility with PI as they are frequently blended together to prepare membranes by the nonsolvent-induced phase separation method.[34,35] Through ALD, PI is uniformly deposited on the pore wall throughout the PES membrane, forming a three-dimensionally interconnected structure wrapping the entire skeleton of the PES membrane. The effective pore size and the separation properties of the PES membranes can be tuned in a relatively wide window by changing the ALD cycle numbers. Furthermore, the deposition of PI evidently enhances the mechanical and thermal stability of the PES membranes.

Experimental Section

Materials

PES flat membranes in the shape of round disks with a diameter of 25 mm (Supor® Membrane, Pall) were used as substrates for ALD. The PES membrane has a nominal pore size of 100 nm according to the supplier and its thickness is determined to be ~132 μm. Pyromellitic dianhydride (PMDA, J&K Scientific) and ethylenediamine (EDA, Sigma-Aldrich) with a purity of ≥99.5% were used as precursors for the ALD of PI. Nitrogen with an ultrahigh purity (99.999%) was used as both the precursor carrier and the sweeping gas for purging. Monodispersed colloidal silica nanospheres with a diameter of 23 nm as determined by dynamic light scattering, purchased from Sigma-Aldrich with a concentration of 40 wt %, were diluted with water and used to measure the retention of the membranes. Purified water with a conductivity of 6 μS/cm was in-house prepared through a reverse osmosis process and used throughout this study.

ALD of PI on PES membranes

PES membranes were positioned in the chamber which was heated to 160°C of a homemade hot-wall ALD reactor. The ALD process was commenced once the chamber was pumped to reach a vacuum of ~2 torr. Both PMDA and EDA were stored in stainless cylinders. Considering the low vapor pressure and high evaporation temperature of PMDA, we maintained the storage cylinder of PMDA at 155°C and set the deposition temperature at 160°C to prevent the condensation of PMDA. EDA was much more volatile than PMDA and it was stored at room temperature. The PMDA and EDA vapors were alternatively pulsed into the ALD chamber by the carrier nitrogen gas at a flow rate of 50 sccm. The pulse duration of PMDA and EDA was 1 and 0.05 s, respectively. After pulse, PMDA and EDA were held in the chamber for 8 and 3 s, respectively, allowing the PES membranes to be sufficiently exposed by each precursor. Nitrogen was subsequently purged into the chamber at the flow rate of 50 sccm for 40 and 15 s after the pulse of PMDA and EDA, respectively, to sweep away the unadsorbed/unreacted precursors and by-products formed during the reaction between the precursors. The pulse, exposure, and purging duration for PMDA were set longer than that of EDA to allow the bulky and less volatile PMDA molecules to have adequate time to overcome the diffusion problems. Such a sequence of operations of "PMDA pulse/exposure/N_2 purge/EDA pulse/exposure/N_2 purge" is termed as one ALD cycle and all these operations are automatically controlled via fast valves. A schematic diagram of the ALD device is shown in Figure 1. We repeated the ALD cycle for different times up to 3000.

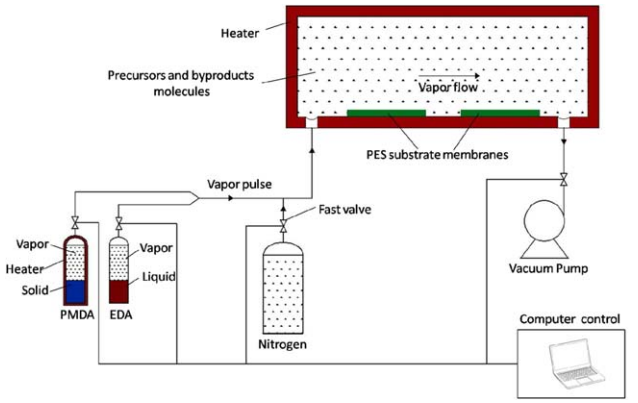

Figure 1. The schematic diagram (not to scale) of the ALD device used to deposit PI on PES membranes.

[Color figure can be viewed in the online issue, which is available at wileyonlinelibrary.com.]

Characterizations

The morphology of membrane samples were observed by a Hitachi S4800 field emission scanning microscope operated at 5 kV. Prior to SEM observation, the samples were first sputtering-coated with a thin layer of Pt/Pd alloy to enhance the conductivity. The distribution of the nitrogen element across the PI-deposited PES substrate membrane was obtained from an Oxford INCA 350 energy dispersive x-ray microanalysis system (EDX) coupled to the SEM and operated at 20 kV. The pore-size distribution and the mean pore size of PES membranes subjected to different ALD cycles were analyzed based on at least 100 pores randomly picked up from the SEM images using an image analysis program (NanoMeasurer). The Fourier transformation infrared (FTIR) spectra of membrane samples were obtained from a Nicolet 8700 FTIR spectrometer in the attenuated total reflection mode (32 scans, 4 cm^{-1}). To hydrolyze PI deposited on PES membranes, membranes with different ALD cycles were separately immersed in 10 wt % aqueous sodium hydroxide (NaOH) solutions at room temperature for 15 h. The content of total organic carbon (TOC) and total nitrogen (TN) of these solutions in which the membranes were immersed were determined by a Multi 3000 TOC/TN analyzer (Analytik Jena AG). The mechanical properties of membranes were

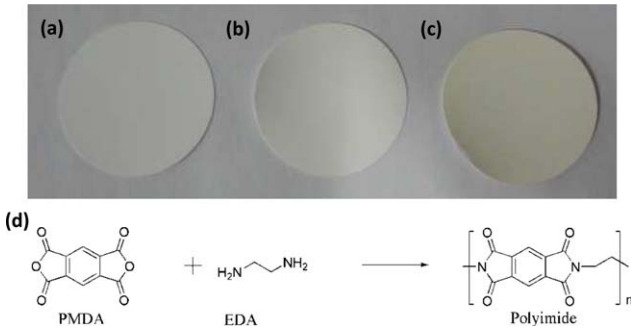

Figure 2. The photographs of the neat PES membrane (a) and the PES membrane subjected to 1000 cycles (b) and 3000 cycles (c), and the equation of the reaction between EDA and PMDA producing PI involved in the ALD process.

[Color figure can be viewed in the online issue, which is available at wileyonlinelibrary.com.]

measured on an electronic tensile tester (CMT-6203, Shenzhen Sans Test Machine Co.) with a tensile rate of 2 mm/min. The samples were prepared in the dimension of 8 × 15 mm^2. For each membrane, we tested three samples and the averaged value of the tensile strength was reported. Membranes were also immersed in water and ultrasonicated at a power of 100 W for 10 min. Differential scanning calorimetry (DSC) analysis of PES membranes with different ALD cycles was performed on a TA TG449F thermal analyzer in the atmosphere of 2:1 N_2/O_2 at a heating rate of 10°C/min from 30 to 400°C. In addition, these membranes were also placed in a furnace and heated to 230°C from room temperature within 20 min and maintained at this temperature for 30 min. Then, membranes were naturally cooled down to room temperature and their structures were checked to assess their thermal resistance.

The water flux and the retention of 23-nm silica of neat and deposited PES membranes were determined using a stirred filtration cell (Amicon 8010, Millipore) at a pressure of 0.01 MPa. The silica solution was diluted for 2500 times with water and then used for retention evaluation. The retention rates were obtained by comparing the concentrations of Si element in the feed and permeate solutions. Silicon concentrations were tested by an inductive coupled plasma emission spectrometer (Optima 7000DV, PerkinElmer).

Results and Discussion

Confirmation of the deposition of PI on PES membranes

We placed PES membranes into the ALD reactor and PMDA and EDA vapors were alternatively pulsed into the reaction chamber. The deposition was performed at the temperature of 160°C as the PMDA vapor is prone to be condensed in the chamber and pipelines at temperatures lower than 150°C and causes clogging problems.[23] PES has a glass transition temperature as high as 230°C and the PES membrane is expected to maintain its structural stability at the moderate deposition temperature of 160°C. The PES membrane after deposition at a cycle number lower than 2000 exhibits no noticeable change and its original white color is preserved (Figures 2a, b). After 3000 ALD cycles, the membrane turns to be yellowish as shown in Figure 2c. This white to yellowish change in color implies that new substance is formed in the membrane. As the reaction between PMDA and EDA can lead to either PI or polyamic acid (PAA),[36,37] we used FTIR analysis to identify the formed substance is PI or PAA. The IR spectra of PES membranes with different ALD cycles were shown in Figure 3. We observed three new peaks at the wave number of 1770, 1710, and 1389 cm^{-1} which can be designated to the asymmetrical and symmetrical stretching vibration of C═O bonds, and the stretching vibration of C─N bonds, respectively. However, the characteristic peak of PAA centered at 1640 cm^{-1} (Ref. 37) could not be observed in the spectra of all PI membranes subjected to various ALD cycles up to 3000. In addition, the IR spectrum implies that the deposited membrane does not contain any unreacted monomers of PI as no characteristic peaks of anhydride (1806 and 1860 cm^{-1})[23] or amine (3300–3500 cm^{-1})[38] can be observed. Therefore, we concluded that PI rather than PAA was formed in the PES membrane through the ALD process and the yellowish color of the 3000-cycles-deposited membrane was due to the formation of relatively thick layer of PI (which is in yellow color in bulk). The reaction between PMDA and EDA directly leading to PI is shown in Figure 2d. By comparing the IR spectra of PES membranes with different PI ALD cycles, we found that the higher the ALD cycle numbers, the stronger the intensity of the PI characteristic peaks. It suggests that the thickness of the PI layer increases with the number of ALD cycles. Moreover, the characteristic peaks of PES, for example, the peak at 1230 cm^{-1}(═C─O─C═), 1140 and 1099 cm^{-1} (S═O), 1573 cm^{-1}, and 1480 cm^{-1}(the vibration of benzene skeleton)[39] became progressively weaker with increasing ALD cycle numbers. This is another indicator that higher ALD numbers produce thicker layers of PI whose shielding effect weakens the penetration depth into the PES substrate of IR signals. The deposition of PI on PES substrate membranes can also be probed by EDX mapping. As shown in Figure 4, signals of nitrogen element originated from deposited PI are present throughout the entire cross section of the PES membrane subjected to 3000 cycles, indicating the full coverage of PI on PES membranes.

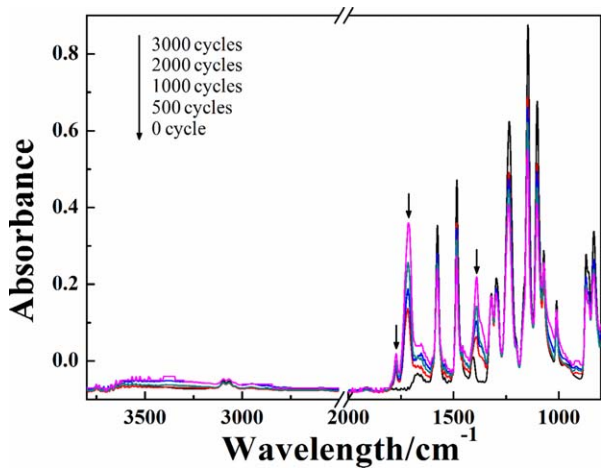

Figure 3. The FTIR spectra of PES membranes subjected to different ALD cycles.

[Color figure can be viewed in the online issue, which is available at wileyonlinelibrary.com.]

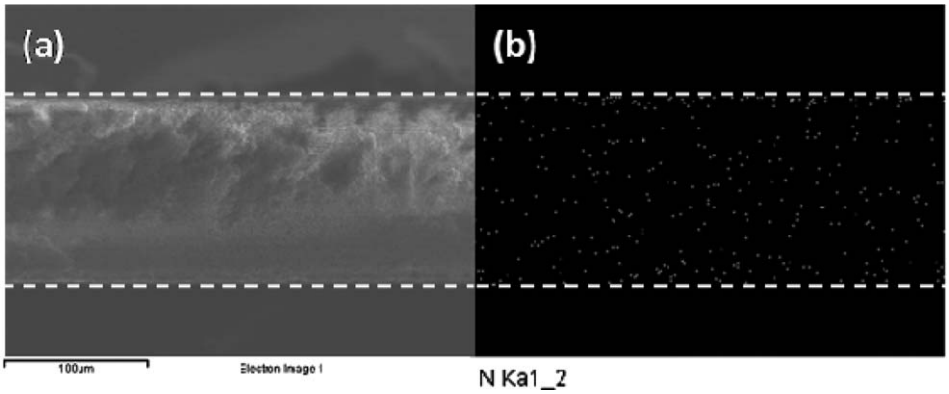

Figure 4. The cross-sectional SEM image of a PES membrane subjected to 3000 cycles of PI ALD (a) and the corresponding EDX map (b) showing the distribution of nitrogen element.

PI can also be deposited on various substrates by conventional vapor deposition polymerization (VDP). VDP seems similar to ALD as they both start with the same precursors and are operated under vacuum at elevated temperatures. However, they are qualitatively different. In the ALD process, the two precursors are separately pulsed into the reaction chamber and their reaction only occurs on the substrate surface (including pore walls) and consequently PI layers are conformally deposited along the surface and pore walls. In contrast, in the VDP process which is a type of CVD, the two precursors are simultaneously introduced into the reaction chamber and the reaction between the precursors takes place immediately when they get contacted in the free volume of the chamber. Primary particles of PI form in the free space of the chamber and precipitate on the top surface of the substrate membrane.[40,41] As a result, pores inside the substrate membrane are free of PI and are not modified. Moreover, VDP needs to be operated under the conditions of considerably high vacuum and temperatures and produces PAA rather than PI. Thermal annealing at even higher temperatures, for example, 300°C, is required to convert PAA to PI.[36,37] Therefore, VDP is not suitable to deposit PI on most polymeric substrates including PES we are using here as they cannot withstand such a high deposition temperature. To have a homogenous modification to porous membranes by the deposition of PI, it is technically easier and more suitable to use the ALD method.

The study of growth process of PI deposition

The ALD of PI on PES substrate membranes is performed in the cyclic mode and one cycle of deposition includes four steps. PMDA vapor is first pulsed into the ALD chamber and forms a monolayer of adsorbed PMDA molecules on the pore wall of the PES membranes. The unadsorbed PMDA molecules are purged out the chamber by nitrogen sweeping in the second step. The second precursor, EDA, is subsequently pulsed into the chamber and reacts with the PMDA previously adsorbed on the pore wall, producing one single molecular layer of PI. In the last step, nitrogen is purged into the chamber again to sweep the unreacted EDA and the by-product (H_2O) of the reaction between PMDA and EDA out the chamber, thus finishing one cycle of ALD of PI. Such cycles repeat for preset numbers to produce a PI layer with a desired thickness. To investigate the growth mode of PI deposition on the PES membrane, we analyzed the weight gain of PES membranes subjected to various ALD cycles. We first directly compared the weight change before and after ALD and found that the weight gain was very minor as the 3000-cycles-deposited membrane gained additional weight of ~3.6% and the 500-cycles-deposited membrane showed no measurable weight gain. Such minor weight gains are not reliable to be directly used to analyze the growth of PI at different ALD cycles. Alternatively, we turned to an indirect method. In this method, the PI-deposited PES membranes were immersed in NaOH aqueous solutions for 15 h to completely decompose the deposited PI, and the TOC content in the solution was measured to assess the amount of deposited PI. As shown in Figure 5, there is a near linear increase of TOC content with the increasing of ALD cycle numbers. The TOC content increased from only 5 mg/L for the neat PES membrane to 21.9, 94.3, and 214.5 mg/L for the membranes with 500, 1500, and 3000 ALD cycles, respectively. Because PI can be fully depolymerized[42] while PES keeps intact in basic conditions, the TOC content in the solution where the membrane is immersed is completely resulted from the depolymerized products of PI. Therefore, the TOC level directly indicates the weight gain because of the deposition of PI if we subtract the slight TOC content produced by the neat PES membrane. Such a linear relationship between the cycle number and the weight gain reveals

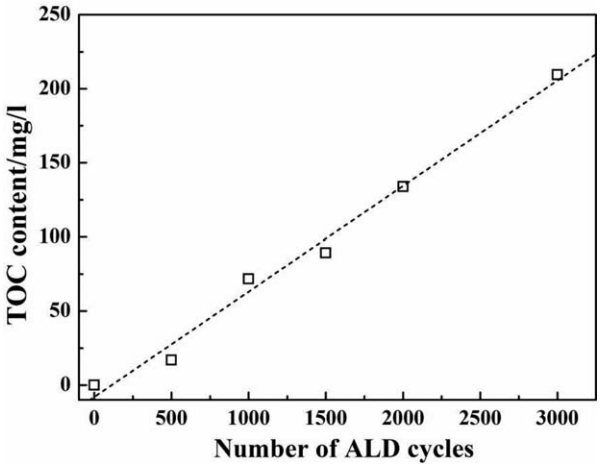

Figure 5. The change of TOC contents in the depolymerized solutions of PES membranes subjected to different ALD cycle numbers.

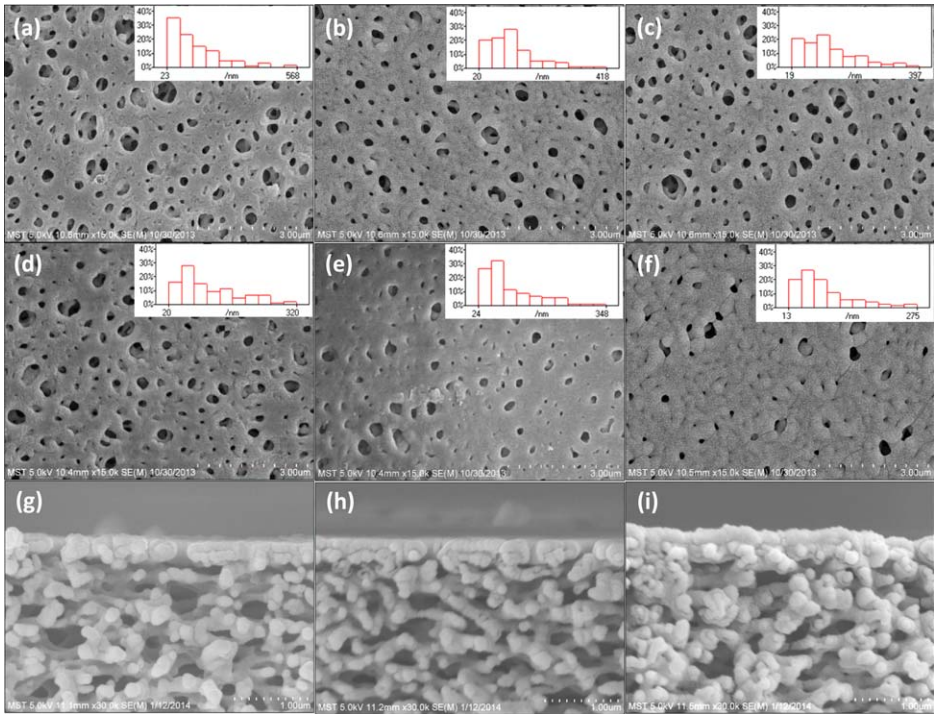

Figure 6. The surface SEM images of PES membranes before (a) and after PI deposition with 500 (b), 1000 (c), 1500 (d), 2000 (e), and 3000 (f) ALD cycles. The cross-sectional SEM images of PES membranes subjected to 0 cycle (g), 1000 cycles (h), and 3000 cycles (i).

The inset in each image is the bar chart of pore-size distribution of the corresponding membrane. [Color figure can be viewed in the online issue, which is available at wileyonlinelibrary.com.]

that the deposition of PI on PES membrane follows a traditional cyclic ALD growth pattern. Moreover, a certain amount of nitrogen reflected as TN can also be detected in the NaOH solution used to treat PI-deposited PES membranes whereas no TN can be detected from the solution of the neat PES membrane. The presence of nitrogen in the solution which is originated from the nitrogen-containing products formed during the PI depolymerization confirms the successful deposition of PI on PES membrane. Unfortunately, as the TN content from the PES membranes subjected to ALD cycles is low, we are unable to correlate a reliable relationship between the TN contents and the weight gains of different ALD cycles as we correlated the TOC contents with weight gains.

The morphology of PI-deposited PES membranes with varying cycles

We examined the surface morphology of PES membranes with different numbers of PI ALD cycles by SEM. As shown in Figure 6a, there are many roughly circular pores with pore sizes widely scattering in the range approximately from 20 to 570 nm on the surface of the neat PES membrane. After ALD deposition of PI up to 3000 cycles, the PES membrane mainly maintains its porous nature with circular pores present on the membrane surface, and there is a reducing trend for the pore sizes and the pore densities with increasing cycle numbers (Figures 6b–f). The reduction in the pore size and pore density is more pronounced at high ALD cycles, for example, 2000 and 3000 cycles (Figures 6e, f). For a better investigation on this change in the pore size with ALD cycle numbers, we analyzed the pore-size distribution and the mean pore size based on the SEM images. The pore-size distribution is inset in each corresponding SEM image. Generally, higher ALD cycle numbers lead to smaller mean pore sizes and largest pore sizes. Figure 7 exhibits the change of the mean pore size with the number of ALD cycles, which reveals a nearly linear reduction of mean pore sizes with cycle numbers. For instance, the mean pore size of the neat PES membrane is 136 nm, and it reduces to 124, 100, and 80 nm after 1000, 2000, and 3000 ALD cycles, respectively. This linear shrinkage in the mean pore size further reveals that PI is progressively coated on the pore walls of the PES membrane via surface growth with almost an identical growth rate. In addition, cross-sectional SEM images (Figures 6g–i) reveal that the symmetric porous structure of the neat PES membrane is preserved and there is

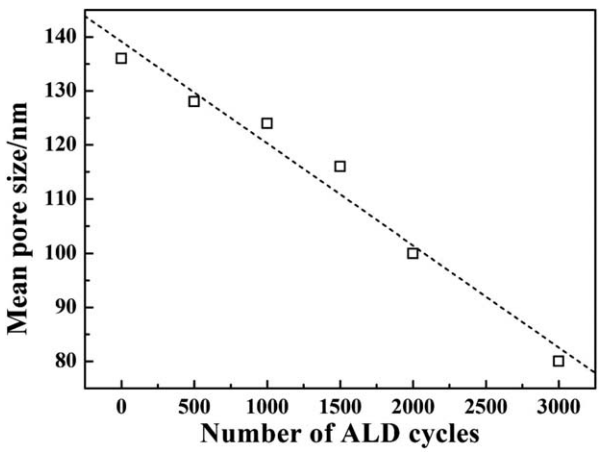

Figure 7. The change of the mean pore size of PES membranes with the number of ALD cycles.

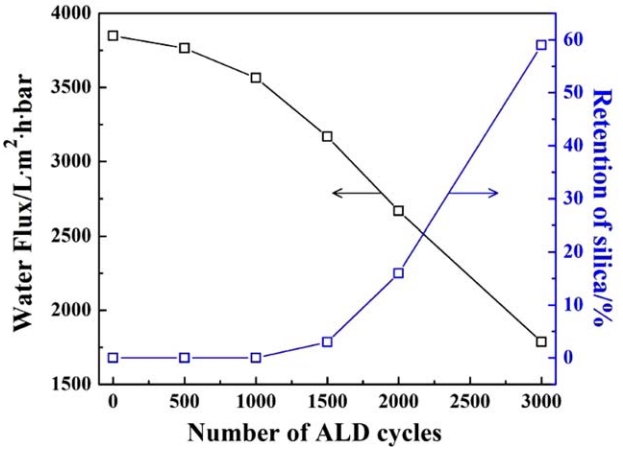

Figure 8. The change of the PWF and the retention to 23-nm silica nanospheres of PES membranes with the number of ALD cycles.

[Color figure can be viewed in the online issue, which is available at wileyonlinelibrary.com.]

no an additional PI layer forming on the top surface of the PES membrane after PI ALD with a cycle number up to 3000. Because of the self-limiting nature of the ALD reactions between vaporized precursors PI deposition occurs throughout the entire thickness of the PES membrane, producing a conformal layer of PI completely wrapping the skeleton of PES. In contrast, the VDP technique produces a dense PAA layer on the top surface of the substrate membrane as PAA does not deposit along the wall of pores in the interior of the membrane, producing a bilayered composite structure.[36] Therefore, VDP does not have the possibility to progressively tune the pore size of the substrate membrane. We are aware of that the above analysis on the pore size is based on the surface pores of the membranes rather than "effective" pores dictating the permselectivity of the membrane; however, it also demonstrates that ALD deposition of PI is capable of adjusting the pore size of PES membranes in a highly controlled and continuous manner.

The tunability of filtration properties of PES membranes by PI ALD

We then investigate the influence of the deposited PI on the water flux and retention of the PES membranes. As shown in Figure 8, pure water flux (PWF) is continuously declined with the increase of PI ALD cycle numbers. PWF is reduced from 3850 L/(m^2 h bar) for the neat PES membrane to 3565 L/(m^2 h bar) after ALD deposition for 1000 cycles, and is further reduced to 1780 L/(m^2 h bar) at a cycle number of 3000. Simultaneously, with the decline of flux, there is a remarkable improvement of the retention performance of the membrane with rising ALD cycle numbers. For instance, the neat PES membrane shows a negligible retention rate of 0.8% to monodispersed silica nanospheres with a diameter of 23 nm. In contrast, the retention rate is increased to 15% and 60% after PI ALD for 2000 and 3000 cycles, respectively. Therefore, there is about over 60 times increase in retention at the expense of 54% decline in water flux after the PES membrane is deposited by PI for 3000 cycles. As we discussed earlier, the membrane only gained a ~3.6% additional weight after PI ALD for 3000 cycles, revealing the ultrathin nature of the deposited PI layer and the preservation of the high porosity of the neat PES membrane. Consequently, the amplitude of the flux decrease was much less than that of the increase of retention rate of the PES membrane after PI ALD. The decrease in flux and the increase in retention with the rising ALD cycle numbers are due to the progressive reduction of the pore size as higher ALD cycle numbers lead to thicker deposited PI layers and consequently a smaller effective pore size. As the water flux and retention vary with cycle numbers in a relatively wide range, the ALD deposition of PI can be used as an efficient and flexible method to tune the separation properties of PES membranes to fit different applications. One may argue that heating during the ALD process may also play a role in changing filtration performances of the PES membrane. To investigate the role of the heating treatment, we treated PES membranes at 160°C (which is the deposition temperature we used in this work) in the ALD chamber without pulsing precursors for 56 h (corresponding to the period of time of 3000 ALD cycles) and measured the PWF of the heated PES membrane. We found that the heated PES membrane preserved its initial water flux. In contrast, as we shown in Figure 8, ALD for 3000 cycles significantly reduced the flux to less than half of the initial flux of the PES membrane. Therefore, we concluded that heating during ALD does not influence the filtration performances of PES membrane, and PI deposition is the dominating factor in tuning the performance of the PES membrane subjected to ALD treatment.

The enhanced thermal resistance of the PI-deposited membranes

As PI typically has a much higher glass transition temperature than PES (~320°C vs. 230°C),[33] the PES membrane with the conformally deposited PI on the pore wall is expected to exhibit enhanced heat resistance. We treated the PES membrane subjected to various ALD cycles at 230°C for 30 min in air. The neat PES membrane, which is originally opaque and in the milky color, turns to transparent after the heat treatment, implying the disappearance of pores in the PES membrane. SEM observation reveals that the surface of the heated PES membrane is completely nonporous (Figure 9a), which is in vivid contrast with the surface morphology of the membrane before heating (Figure 6a). The loss of pores in the membrane is due to the thermal deformation of the PES skeleton and the collapse of the void structure in the original PES membrane. In the DSC curve of the neat PES membrane, there is a strong exothermic peak around 230°C indicating that the glass transition occurs around this temperature (Figure 10a). After ALD of PI for 1000 cycles, the PES membrane predominantly preserves its macroscopic structure and color. SEM examination shows that its porous structure is mainly maintained although some small pores present on the surface before heating disappear (Figure 9b vs. Figure 6c). Therefore, we conclude that PI deposition for 1000 cycles significantly enhances the heat resistance of the PES membrane. An exothermic peak can still be observed on the DSC curve of the PES membrane subjected to 1000 and 2000 ALD cycles (Figures 10b, c), demonstrating that glass transition still happens to this membrane. Therefore, the enhanced heat resistance should be attributed to the presence of a conformal layer of PI wrapping the entire skeleton of the PES membrane, preventing the collapse of the PES framework which is in the threshold of glass transition. For the PES membrane with a PI ALD

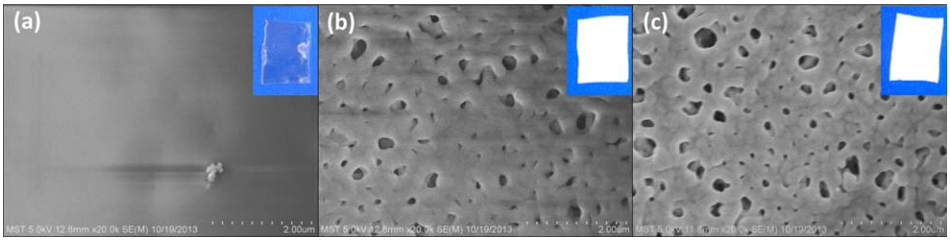

Figure 9. The surface SEM images of PES membranes subjected to 0 (a), 1000 (b), and 3000 (c) ALD cycles and a thermal treatment at 230°C for 30 min.

The inset in each image shows the photograph of the corresponding thermally treated membranes. [Color figure can be viewed in the online issue, which is available at wileyonlinelibrary.com.]

for 3000 cycles, it safely survives the heat challenge at 230°C. Its macroscopic structure and color are completely kept unchanged and its microstructure as revealed by SEM does not have any noticeable difference compared to that of the membrane before heating (Figure 9c vs. Figure 6f). Interestingly, its DSC curve does not show any exothermic peak (Figure 10d), implying that a thicker PI deposition layer completely suppresses the glass transition of PES chains. Consequently, the thermal stability of the membrane is remarkably enhanced.

The enhanced mechanical performance of the PI-deposited PES membranes

The PI-deposited PES membranes are expected to have enhanced mechanical stability because PI has a stronger mechanical strength than PES. We measured the mechanical properties of neat and PI-deposited PES membranes. As shown in Figure 11, the PI-deposited PES membranes exhibit a stronger tensile strength and a reduced elongation than the neat one, indicating that the membrane becomes stronger and tougher after PI deposition. The tensile strength and the tensile yield stress of the neat PES membrane is 5.5 and 4.5 MPa, respectively, which is increased to 6.1 and 5.2 MPa, respectively, after PI deposition for 1000 cycles. Further increasing the cycle number to 3000 leads to an even higher tensile yield stress of 5.6 MPa and a tensile strength of 5.8 MPa which is lower than that of the 1000-cycle-deposited membrane but still higher than the neat PES membrane. To further confirm the enhanced strength of the PES membranes by PI deposition, we immersed the three membranes in water and challenged them with ultrasonication oscillation at the power of 100 W. After ultrasonication for 10 min, water in which the neat PES membrane is immersed turned turbid because the membrane had been completely broken down into small debrises which were temporarily suspended in water (Figure 12a). Moreover, SEM examinations reveal that there are also many cracks in the membrane debris (Figure 12b). In contrast, the membranes subjected to ALD PI for 1000 and 3000 cycles maintained their original structural integrity at the macroscopic level. However, a few cracks could also be observed on the surface of the membrane with a cycle number of 1000 (Figure 12b), whereas the 3000-cycles-deposited PES membrane survived the ultrasonication as no cracks could be observed on its surface (Figure 12c). This ultrasonication challenge also demonstrates that the enhanced mechanical robustness of the PES membrane, which should be attributed to the uniform and tight adhesion of the deposited PI layer on the PES substrate membrane. The deposition of PI does not only occur on the top surface or near-surface region of the PES membrane like other deposition methods, for example, CVD. Instead, PI deposition takes place throughout the entire membrane with the thorough penetration of the vaporized ALD precursors into the porous interior of the PES membrane, producing a three-dimensionally interconnected network of PI layer along the skeleton of the PES substrate membrane. Because of the

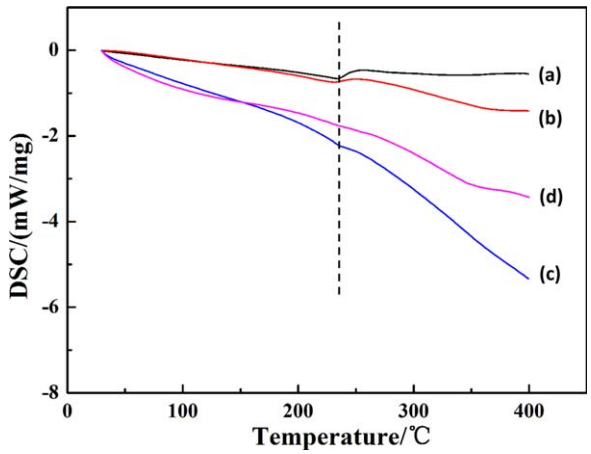

Figure 10. The DSC curves of PES membranes subjected to 0 (a), 1000 (b), 2000 (c), and 3000 (d) cycles.

[Color figure can be viewed in the online issue, which is available at wileyonlinelibrary.com.]

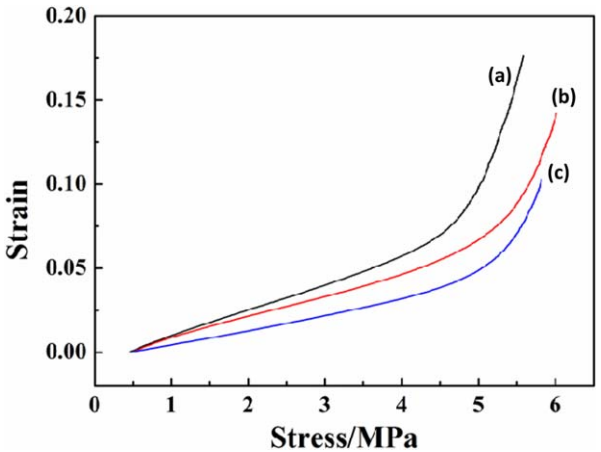

Figure 11. The stress–strain curves of PES membrane subjected to 0 (a), 1000 (b), and 3000 (c) ALD cycles.

[Color figure can be viewed in the online issue, which is available at wileyonlinelibrary.com.]

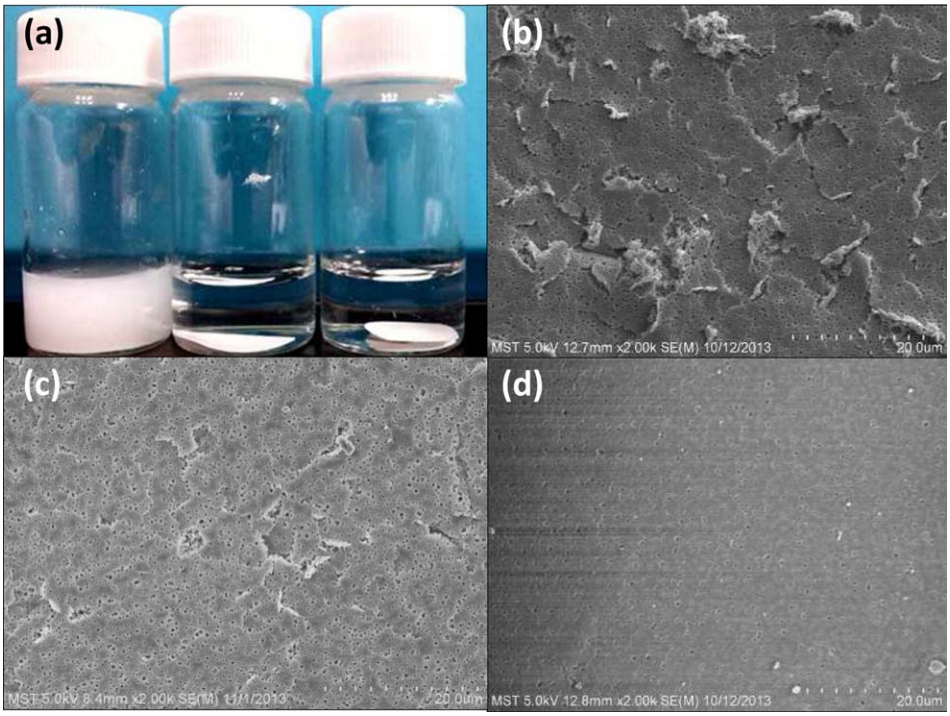

Figure 12. The photograph of membranes immersed in water and challenged by ultrasonication for 10 min (a), and the SEM image of the ultrasonicated PES membranes subjected to 0 (b), 1000 (c), and 3000 (d) ALD cycles. The three bottles in (a) from left to right contain the neat PES membrane and the membrane subjected to 1000 and 3000 ALD cycles, respectively.

[Color figure can be viewed in the online issue, which is available at wileyonlinelibrary.com.]

interlocking effect of the PI layer with the PES substrate, the enhancement of the mechanical strength is more pronounced.[16,18] As a result, we did not observe any delamination, which occurs frequently in two-dimensionally layered composite structures, of the ALD-deposited membranes in both the tensile test and the ultrasonication challenge.

Conclusions

We demonstrate the controllable coating of PI along the pore wall of PES microporous membranes by ALD using PMDA and EDA as the precursors. The precursors are separately pulsed into the ALD reactor to grow a conformal PI layer in the membranes uniformly. The pore size of the PES membranes is progressively reduced with increasing ALD cycle numbers, leading to the continuous rise in rejection rate and drop in permeability. The increase of rejection rate with rising ALD cycles is more pronounced than the drop of permeability, for example, there is an over 60 times increase in the rejection rate for the PES membrane subjected to PI ALD for 3000 cycles whereas its flux is only reduced by 54%. Moreover, the PI-deposited PES membranes survive thermal treatment up to 230°C and a harsh ultrasonication challenge because of their remarkably enhanced thermal resistance and mechanical strength. This significant improvement in thermal and mechanical performance is due to a uniform and tight PI layer wrapping the skeleton of the porous PES membrane.

Acknowledgment

This work is financially supported by the Natural Science Research Program of the Jiangsu Higher Education Institutions (13KJA430005), the National Natural Science Foundation of China (21176120), the Jiangsu Natural Science Funds for Distinguished Young Scholars (BK2012039), and the Project of Priority Academic Program Development of Jiangsu Higher Education Institutions (PAPD).

Literature Cited

1. Shannon MA, Bohn PW, Elimelech M, Georgiadis JG, Marinas BJ, Mayes AM. Science and technology for water purification in the coming decades. *Nature*. 2008;452:301–310.
2. Strathmann H. Membrane separation processes: current relevance and future opportunities. *AIChE J*. 2001;47:1077–1087.
3. Rungta M, Zhang C, Koros WJ, Xu LR. Membrane-based ethylene/ethane separation: the upper bound and beyond. *AIChE J*. 2013;59:3475–3489.
4. Albo SE, Broadbelt LJ, Snurr RQ. Multiscale modeling of transport and residence times in nanostructured membranes. *AIChE J*. 2006;52:3679–3687.
5. Hinds BJ, Chopra N, Rantell T, Andrews R, Gavalas V, Bachas LG. Aligned multiwalled carbon nanotube membranes. *Science*. 2004;303:62–65.
6. Nair RR, Wu HA, Jayaram PN, Grigorieva IV, Geim AK. Unimpeded permeation of water through helium-leak-tight graphene-based membranes. *Science*. 2012;335:442–444.
7. Nunes SP, Car A. From charge-mosaic to micelle self-assembly: block copolymer membranes in the last 40 years. *Ind Eng Chem Res*. 2013;52:993–1003.
8. Keskin S, Sholl DS. Screening metal-organic framework materials for membrane-based methane/carbon dioxide separations. *J Phys Chem C*. 2007;111:14055–14059.
9. Kanezashi M, O'Brien-Abraham J, Lin YS, Suzuki K. Gas permeation through DDR-type zeolite membranes at high temperatures. *AIChE J*. 2008;54:1478–1486.
10. Wang NX, Zhang GJ, Ji SL, Fan YQ. Dynamic layer-by-layer self-assembly of organic-inorganic composite hollow fiber membranes. *AIChE J*. 2012;58:3176–3182.
11. Rana D, Matsuura T. Surface modifications for antifouling membranes. *Chem Rev*. 2010;110:2448–2471.

12. Sneh O, Clark-Phelps RB, Londergan AR, Winkler J, Seide TE. Thin film atomic layer deposition equipment for semiconductor processing. *Thin Solid Films*. 2002;402:248–261.
13. Kim H, Lee HBR, Maeng WJ. Applications of atomic layer deposition to nanofabrication and emerging nanodevices. *Thin Solid Films*. 2009;517:2563–2580.
14. Liu MN, Li XL, Karuturi SK, Yoong Tok AI, Fan HJ. Atomic layer deposition for nanofabrication and interface engineering. *Nanoscale*. 2012;4:1522–1528.
15. Li FB, Li L, Liao XZ, Wang Y. Precise pore size tuning and surface modifications of polymeric membranes using the atomic layer deposition technique. *J Membr Sci*. 2011;385:1–9.
16. Xu Q, Yang Y, Wang XZ, Wang ZH, Jin WQ, Huang J, Wang Y. Atomic layer deposition of alumina on porous polytetrafluoroethylene membranes for enhanced hydrophilicity and separation performances. *J Membr Sci*. 2012;415:435–443.
17. Wang QQ, Wang XT, Wang ZH, Huang J, Wang Y. PVDF membranes with simultaneously enhanced permeability and selectivity by breaking the tradeoff effect via atomic layer deposition of TiO_2. *J Membr Sci*. 2013;442:57–64.
18. Li FB, Yang Y, Fan YQ, Xing WH, Wang Y. Modification of ceramic membranes for pore structure tailoring: the atomic layer deposition route. *J Membr Sci*. 2012;397:17–23.
19. George SM. Atomic layer deposition: an overview. *Chem Rev*. 2010; 110:111–131.
20. George SM, Yoon B, Dameron AA. Surface chemistry for molecular layer deposition of organic and hybrid organic-inorganic polymers. *Acc Chem Res*. 2009;42:498–508.
21. Mato K, Kornelius N, Lauri N. Synthesis and surface engineering of complex nanostructures by atomic layer deposition. *Adv Mater*. 2007;19:3425–3438.
22. Ritala M, Leskela M. Atomic layer deposition chemistry: recent developments and future challenges. *Angew Chem Int Ed*. 2003;42: 5548–5554.
23. Putkonen M, Harjuoja J, Sajavaara T, Niinisto L. Atomic layer deposition of polyimide thin films. *J Mater Chem*. 2007;17:664–669.
24. Salmi LD, Puukilainen E, Vehkamaki M, Heikkila M, Ritala M. Atomic layer deposition of Ta_2O_5/polyimide nanolaminates. *Chem Vap Deposition*. 2009;15:221–226.
25. Mittal KL. *Polyimides: Synthesis, Characterization, and Applications*. New York: Plenum Press, 1984.
26. Liu Y, Wang R, Chung TS. Chemical cross-linking modification of polyimide membranes for gas separation. *J Membr Sci*. 2001;189:231–239.
27. Heuchel M, Hofmann D. Molecular modelling of polyimide membranes for gas separation. *Desalination*. 2002;144:67–72.
28. White LS. Transport properties of a polyimide solvent resistant nanofiltration membrane. *J Membr Sci*. 2002;205:191–202.
29. Darvishmanesh S, Degreve J, Van der Bruggen B. Performance of solvent-pretreated polyimide nanofiltration membranes for separation of dissolved dyes from toluene. *Ind Eng Chem Res*. 2010;49:9330–9338.
30. Qiao XY, Chuang TS. Diamine modification of P84 polyimide membranes for pervaporation dehydration of isopropanol. *AIChE J*. 2006; 52:3462–3472.
31. Daraei P, Madaeni SS, Ghaemi N, Khadivi MA, Astinchap B, Moradian R. Enhancing antifouling capability of PES membrane via mixing with various types of polymer modified multi-walled carbon nanotube. *J Membr Sci*. 2013;444:184–191.
32. Lin JY, Zhang RX, Ye WY, Jullok N, Sotto A, Bruggen BV. Nano-WS_2 embedded PES membrane with improved fouling and permselectivity. *J Colloid Interface Sci*. 2013;396:120–128.
33. Kapantaidakis GC, Koops GH. High flux polyethersulfone-polyimide blend hollow fiber membranes for gas separation. *J Membr Sci*. 2002;204:153–171.
34. Kapantaidakis GC, Kaldis SP, Dabou XS, Sakellaropoulos GP. Gas permeation through PSF-PI miscible blend membranes. *J Membr Sci*. 1996;110:239–247.
35. Kapantaidakis GC, Koops GH, Wessling M, Kaldis SP, Sakellaropoulos GP. CO_2 plasticization of polyethersulfone/polyimide gas-separation membranes. *AIChE J*. 2003;49:1702–1711.
36. Spassova E. Vacuum deposited polyimide thin films. *Vacuum*. 2003; 70:551–561.
37. Yanagisita H, Kitamoto D, Haraya K, Nakane T, Tsuchiya T, Koura N. Preparation and pervaporation performance of polyimide composite membrane by vapor deposition and polymerization (VDP). *J Membr Sci*. 1997;136:121–126.
38. Yao HY, Zhang Yh, Liu Y,You KY, Liu SY, Liu BJ, Guan SW. Synthesis and properties of cross-linkable high molecular weight fluorinated copolyimides. *J Polym Sci Part A: Polym Chem*. 2014;52: 349–359.
39. Peyravi M, Rahimpour A, Jahanshahi M, Javadi A, Shockravi A. Tailoring the surface properties of PES ultrafiltration membranes to reduce the fouling resistance using synthesized hydrophilic copolymer. *Microporous Mesoporous Mater*. 2012;160:114–125.
40. Detavernier C, Dendooven J, Sree PS, Ludwigc KF, Martensb JA. Tailoring nanoporous materials by atomic layer deposition. *Chem Soc Rev*. 2011;40:5242–5253.
41. Sovan Kumar P, Hyunjung S. Step coverage in ALD. In: Nicola P, Mato K, editors. *Atomic Layer Deposition of Nanostructured Materials*. Weinheim: Wiley-VCH Verlag GmbH & Co. KGaA, 2012:23–40.
42. Thomas RR. Quantification of ionizable functional groups on a hydrolyzed polyimide surface. *Langmuir*. 1996;12:5247–5249.

Manuscript received Jan. 16, 2014, and revision received Apr. 27, 2014.